Research Article | Vol. 11, No. 4 / 1 April 2020 / Biomedical Optics Express 2268
Biomedical Optics EXPRESS

Visualization of blood cell contrast in nailfold capillaries with high-speed reverse lens mobile phone microscopy

GREGORY N. MCKAY,[1] NELA MOHAN,[1] IAN BUTTERWORTH,[2] AURÉLIEN BOURQUARD,[2] ÁLVARO SÁNCHEZ-FERRO,[2] CARLOS CASTRO-GONZÁLEZ,[2] AND NICHOLAS J. DURR[1,*]

[1]*Department of Biomedical Engineering, Johns Hopkins University (JHU), 3400 N. Charles Street, Baltimore, MD 21218, USA*
[2]*Leuko Labs Inc., 8 St. Mary's Street #613, Boston, MA 02215, USA*
[*]*ndurr@jhu.edu*
http://durr.jhu.edu

Abstract: Quantification of optical absorption gaps in nailfold capillaries has recently shown promise as a non-invasive technique for neutropenia screening. Here we demonstrate a low-cost, portable attachment to a mobile phone that can resolve optical absorption gaps in nailfold capillaries using a reverse lens technique and oblique 520nm illumination. Resolution <4μm within a 1mm^2 on-axis region is demonstrated, and wide field of view (3.5mm × 4.8mm) imaging is achieved with resolution <6μm in the periphery. Optical absorption gaps (OAGs) are visible in superficial capillary loops of a healthy human participant by an ~8-fold difference in contrast-to-noise ratio with respect to red blood cell absorption contrast. High speed video capillaroscopy up to 240 frames per second (fps) is possible, though 60fps is sufficient to resolve an average frequency of 37 OAGs/minute passing through nailfold capillaries. The simplicity and portability of this technique may enable the development of an effective non-invasive tool for white blood cell screening in point-of-care and global health settings.

1. Introduction

Capillaroscopy, the microscopic evaluation of capillary organization and microvascular blood flow, is a century old technique that has shown value in a variety of clinical fields. The evaluation of nailfold capillary morphology to assess Raynaud's disease and systemic sclerosis is an established clinical technique, capillary tortuosity and blood velocity are significantly correlated with diabetic retinopathy severity, and capillary plexus visibility has been shown to correlate even with seemingly distant disease processes such as schizophrenia [1–5].

Despite its long history, new discoveries and novel applications of nailfold capillaroscopy are still being developed, and renewed interest has recently been spurred by modern microscopy techniques and improved imaging technologies. High speed video capillaroscopy can resolve, track, and quantify optical absorption gaps (OAGs) between red blood cells [6,7] flowing in capillaries, which are typically 150-400μm deep in the nailfold [8]. Evidence that these absorption gaps are caused by white blood cells has been demonstrated in a variety of settings including animal cremaster vasculature and in the retina, as it relates to the blue entopic phenomenon [9–12]. The frequency of OAGs has recently been found to correlate with neutropenic status in cancer patients receiving chemotherapy, opening the door to non-invasive, at-home or point-of-care measurement of white blood cell (WBC) concentration [7,13]. Current invasive methods to measure WBC status require a finger prick or venipuncture, which can subject already immunocompromised cancer patients to increased risk of iatrogenic infection and hospitalization [14]. Additionally, due to the required trained personnel and expensive laboratory equipment for

#382376 https://doi.org/10.1364/BOE.382376
Journal © 2020 Received 4 Nov 2019; revised 21 Mar 2020; accepted 23 Mar 2020; published 30 Mar 2020

Biomedical Optics EXPRESS

a conventional complete blood count, the development of more accessible tools that accomplish similar tasks would be valuable in remote and low-resource settings without access to cytometry labs. Further, the WBC count generally provides a gauge of immune status, and is commonly used in diagnosing infection, cancer, immune suppression, and auto-immune disease [15–18].

The widespread use of mobile phones with increasingly-sophisticated imaging capabilities provides an opportunity for global health tools that can be deployed at wide scales. Camera phones have been developed for applications that include prescribing eyeglasses [19], diagnosing ear infections [20], and screening for anemia [21]. Many mobile phone based portable microscopes have been developed in the last decade [22–26], each with various tradeoffs of complexity, image resolution, and field of view. Recently, Switz *et al.* proposed a simple reverse lens attachment to a mobile phone camera that enables high resolution 1x imaging over a large field of view [27]. The symmetry in this reverse lens approach yields simultaneous satisfaction of the Sine and Herschel conditions, leading to correction of spherical aberration [28]. Further, the additional reversed lens has an identical acceptance angle to the intrinsic mobile phone lens, leading to a wide field of view that utilizes the entire imaging sensor [27].

In this paper, we develop and characterize a portable nailfold capillaroscope attachment for an iPhone X that relies on this reverse lens approach and demonstrate that this technique can resolve optical absorption gaps in human nailfolds *in vivo*. Given prior research demonstrating correlation between nailfold absorption gap frequency and neutropenia [7,13], we envision this approach could enable rapid white blood cell screening in point-of-care applications, including low-income countries, where infection and communicable disease are among the leading causes of death [29,30].

2. Materials and methods

2.1. Reverse lens capillaroscope

The reverse lens iPhone X capillaroscope consists of a detachable, 3D printed housing to hold the external lens and four green LEDs within a battery powered circuit (Fig. 1). The external lens was harvested from an OEM iPhone X widefield rear camera replacement part (SKU #9-AP-3772 [31]). The orientation of this lens was reversed and positioned in contact with the internal mobile phone lens via a 3D-printed housing (printed on Formlabs Form 2). We choose to implement our capillaroscope using the wide-angle camera due to its high numerical aperture (f/# = 1.8), and predicted diffraction-limited resolution of 1.14μm [32]. Four green LEDs (Lighthouse LEDs, 1.8mm, 515-525nm, 20-30° viewing angle) were fastened into the housing at 70° to the optic axis, adjacent to the clear aperture of the reversed lens. The LEDs were wired in parallel to each other, each with 200Ω resistors, and powered by a 3V DC battery (CR2032). The reverse-lens housing was designed to pressure-fit to the raised surface around the rear camera of the iPhone X.

LEDs were aligned with oblique geometry at 70° to enable for bright illumination of the short working distance and to help eliminate specular back reflection. Green light was chosen for two reasons: (1) green light gives high contrast for OAGs, managing the tradeoff between imaging depth and contrast from hemoglobin absorption, and (2) green illumination allows us to exploit the higher spatial sampling frequency of the Bayer filter commonly found in mobile phone cameras.

2.2. Image resolution

Image quality and magnification were measured using a 1952 NBS Imaging Target (Thorlabs, Fig. 2(a)-(d))). The resolution was characterized across the field of view by measuring MTFs from a slanted edge up to 2.55 mm off-axis. After quantitatively assessing the system with the resolution target in air, a microfluidic capillary phantom was fabricated to qualitatively assess the visibility of red blood cells. We used a previously-developed protocol [33] to construct a PDMS

Biomedical Optics EXPRESS

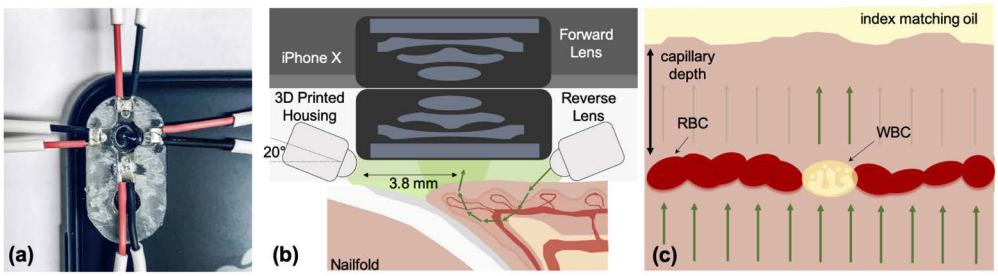

Fig. 1. Reverse lens capillaroscope design. (a) Image of mounted mobile phone capillaroscope prototype, (b) nailfold imaging with reverse lens technique, (c) contrast to red blood cells (RBCs) is generated due to absorption of green light by hemoglobin, leaving white blood cells or plasma gaps appearing bright.

phantom with 20 μm wide capillaries 50 μm below the surface (Fig. 2(e)). The PDMS was doped with Titanium Dioxide and India ink to create reduced scattering and absorption coefficients of 1.7 mm^{-1} and 0.02 mm^{-1} at 520nm respectively, mimicking the optical properties of human skin. Human blood was flowed through this phantom with a syringe pump at physiologically-realistic speeds around $\sim$ 500 μm/s, and imaged with the cell-phone prototype. Since human nailfold capillaries are 150-400μm deep [8], this measurement provides a best-case scenario for visualizing individual blood cells.

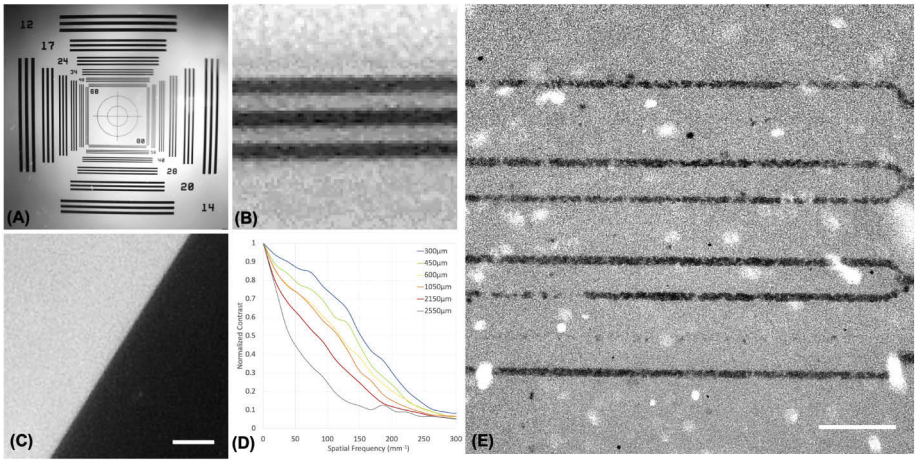

Fig. 2. Capillaroscope resolution characterization. (a) Image of 1952 NBS Imaging Target. Numerical markings have units of line pairs per mm (lp/mm). (b) Magnified region of interest from (a) including three lines at a spatial frequency of 80 lp/mm. (c) Edge spread function used for 2550μm off axis MTF calculation (50μm scale bar). (d) Calculated MTFs for edge spread functions acquired at increasing distance from the optic axis. (e) Image of superficial capillaries in a microfluidic phantom demonstrates resolution of single red blood cell shadows (200 μm scale bar).

2.3. *Nailfold imaging*

Imaging human nailfolds *in vivo* was performed with approval from the Johns Hopkins University Institutional Review Board (IRB00204985). All participants provided written consent before entering the study. Prior to imaging, a drop of mineral oil was placed on the nailfold to help

Biomedical Optics EXPRESS

index match and smooth the tissue surface. Image data were acquired in RAW mode using the image acquisition application VSCO (Visual Supply Company), with the following settings manually fixed: ISO = 125, exposure time = 1/952 seconds, aperture size = f/1.8, and manual focus position = infinity. Video data were acquired using the app FiLMiC (Filmic Entertainment), at 2160 x 3840 pixel image size, with ISO = 200, and exposure time = 1/700 seconds. Though the iPhone X is capable of 240fps, we found that 60fps was sufficient for capturing flowing OAGs, and so this setting was used for all video data presented in this manuscript. Visibility of OAGs was assessed using contrast-to-noise ratio: CNR = $(\mu_b - \mu_c)/\sqrt{\sigma_b^2 + \sigma_c^2}$. Where μ_b and μ_c are the mean and σ_b and σ_c are the standard deviation in a line profile across the background tissue and capillary, respectively. The CNR is typically high due to absorption contrast when red blood cells fill the lumen of the capillary. In the presence of an OAG, the CNR drops to near unity. The CNR was calculated across 5 capillaries in the presence and absence of an OAG.

3. Results

3.1. Image resolution

The image quality was assessed by imaging a resolution target (1952 NBS Imaging Target, Thorlabs, Fig. 2(a)-(b)) and calculating MTFs from edge spread functions taken at different locations across the field of view, using the slanted edge technique (Fig. 2(c)-(d)) [34]. Using the 80lp/mm markings as a fiducial, the magnification of the system was measured to be 1.03x, close to the expected 1x, resulting in a field of view of 3.5mm x 4.8mm.

The resolution of the system was determined to be 3.75μm (on-axis) by identifying and taking the inverse of the spatial frequency at which the normalized contrast drops to 10% (267 mm^{-1}). The iPhone X rear widefield camera has a pixel size of 1.22μm, leading to a sample pixel size of 1.18μm. Assuming the sensor operates with a standard RGGB Bayer pattern color filter, the effective pixel pitch of the green channel in the imaging system is $1.18\sqrt{2} = 1.67\mu$m. Using classical sampling criteria [35], we calculate a predicted maximum resolvable spatial frequency of 299mm^{-1}, and a spatial resolution of 3.34μm. The observed on-axis resolution is close to what is predicted by the Nyquist sampling limit. Resolution worsened as further off-axis MTFs were calculated, however a resolution of 5.2μm was still observed up to 2.55mm off-axis, highlighting the wide field of view capability of this technique, (Fig. 2(d)). The size of the point spread function is similar to the maximum dimension of a red blood cell (6 - 8 μm). We experimentally tested the capability of the system to image individual red blood cells in a microfluidic capillary phantom. One such RAW image of this phantom is demonstrated in Fig. 2(e), where individual red blood cells are visible as absorption shadows ~8 μm across.

3.2. Nailfold imaging

With a drop of mineral oil applied to a human nailfold, RAW images were acquired of capillary loops. Figure 3 demonstrates the ability of the mobile phone capillaroscope to resolve optical absorption gaps *in vivo* in human nailfolds using RAW image acquisition. Figure 3(a)-(b) shows example images of nailfold capillaries separated by approximately 500 ms in time. When red blood cells fill the lumen of the capillary, capillary outlines are dark due to absorption contrast (Fig. 3(c)) and demonstrate an average contrast-to-noise ratio (CNR) of 4.7 (σ = 0.7). Optical absorption gaps (OAGs) between absorbing red blood cells are distinguishable as a decrease in CNR to an average of 0.6 (σ = 0.4), highlighted in Fig. 3(d). Representative line profiles showing the variation in intensity across the capillary with and without an absorption gap are shown in Fig. 3(e).

Biomedical Optics EXPRESS

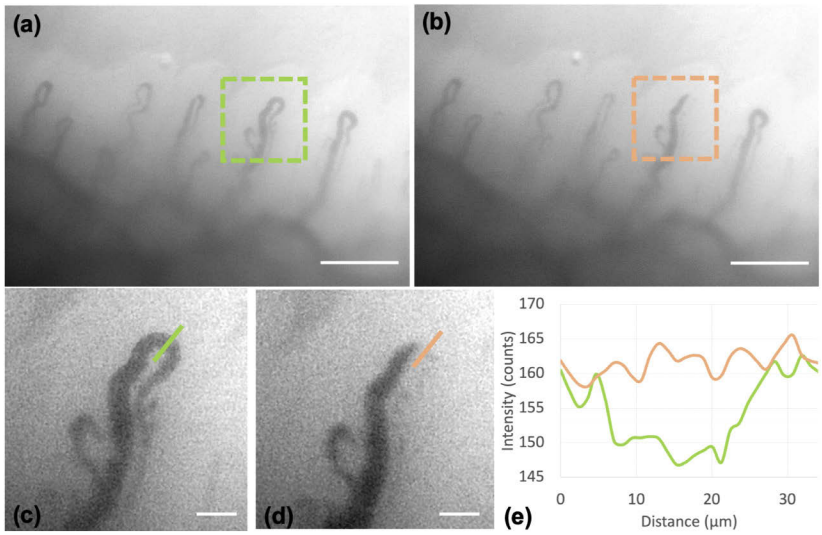

Fig. 3. (a)-(b) Raw nailfold capillary images at different time points (Δt = 500 ms) demonstrate imaging of optical absorption gaps *in vivo*. Scale bars are 250μm. (c)-(d) Boxed regions in (a) and (b), respectively, highlight a flowing absorption gap. Scale bars are 50μm. (e) Representative line profile through green and orange lines highlighted in (c) and (d).

3.3. *High speed video capillaroscopy*

The high speed sensors in the iPhone X allow imaging up to 240fps at 2160 x 3840 resolution. However, the impressive speed and small size of the device are made possible through sophisticated video codecs (H.264 and HEVC) that are lossy compared to RAW image acquisition. We find that, despite this compression, optical absorption gaps are still resolvable in high speed video acquisition. In practice, because we are using a low magnification system and nailfold capillary flow is often 1mm/s or slower [36], we found 60fps imaging was sufficient to capture optical absorption gap flow. At 1mm/s blood cell velocity and 60fps acquisition, we calculate a given blood cell would translate approximately 17μm (14 pixels) per frame, fast enough to capture around 14 images of a single OAG flowing through a capillary loop 200μm in length. Figure 4 shows temporally-separated frames (Δt = 83ms) from a nailfold capillaroscopy video. Overall, we analyzed 9 seconds of video of blood flow through 5 capillaries, and observed an average ± standard deviation frequency of 37 ± 25 OAGs/minute (see Visualization 1). This rate is within the range observed by Bourquard et al. in baseline participants (individuals without neutropenia) [7]. The OAG count per minute, called the "Leuko Index," has been shown to inversely correlate with absolute neutrophil count [7,13]. The average diameter of the absorption gaps observed in this video was 7.6 μm with a standard deviation of 1.9 μm.

The effect of the video compression is particularly visible when examining the background pixel-wise noise present in RAW image acquisition (Fig. 2(b), and Fig. 3(c)-(d)), as compared to the patch-wise noise present in high speed video acquisition Fig. 4(b)-(f). Despite this, optical absorption gaps are still readily visible in the videos (see Visualization 2). Absorption gaps flowing through capillary loops can be temporally tracked (orange arrows, Fig. 4(b)-(f)). Using this approach, the speed of the optical absorption gaps was measured at a mean of 390μm/s with a standard deviation of 106μm/s across five different capillaries.

Biomedical Optics EXPRESS

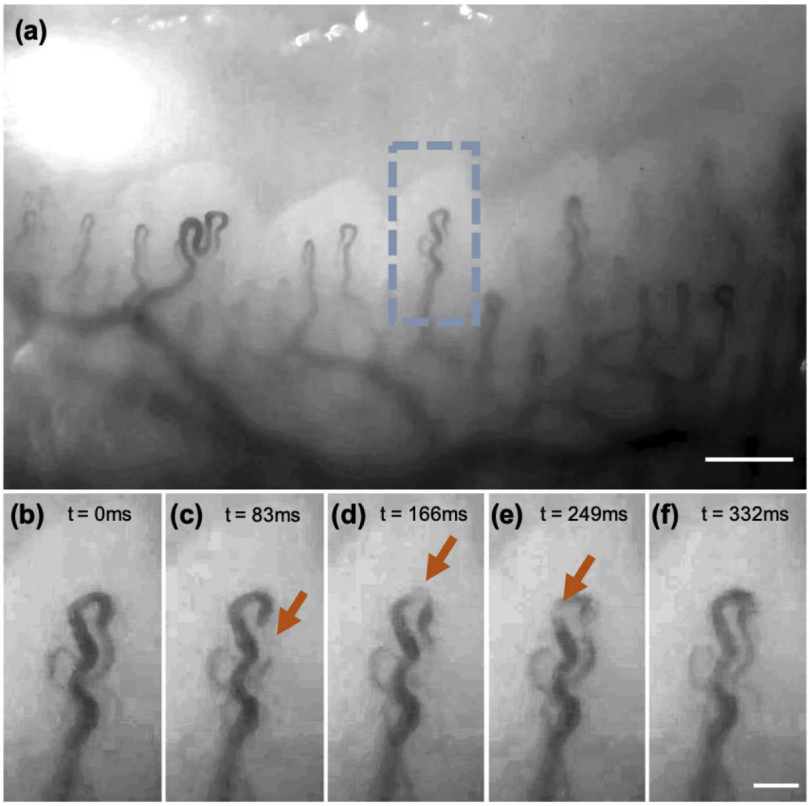

Fig. 4. (a) Wide field of view nailfold capillaroscopy image, 200μm scale bar (see Visualization 1). (b)-(f) Boxed region of interest from (a) with temporally-separated images from a high speed video capillaroscopy acquisition at 60fps. Every 5th frame was selected from the video, with a temporal separation of 83ms. Scale bar is 50μm. (see Visualization 2).

4. Discussion

Our experiments demonstrate that mobile phone capillaroscopy is a promising technique for point-of-care white blood cell (WBC) count screening due to its ability to resolve optical absorption gaps (OAGs). We demonstrate that both RAW image and video acquisition can resolve OAGs, though lossy compression in video introduces additional artifacts. Video information could be used to estimate blood velocity and verify the incompressibility of OAGs to distinguish between WBCs and plasma gaps. This represents a promising avenue for delivering neutropenia or leukocytosis screening in a point-of-care or global health setting because mobile phones are commonly available, compact, battery-powered, and portable. They are powerful, cloud-connected computers, which could enable automated counting of OAGs [13].

Non-invasive absolute neutrophil count (ANC) screening was initially shown possible with a prototype by Bourquard et al. [7]. This prototype demonstrated 5x, 4.2μm resolution, 60 fps imaging with a 1.360 x 1.088 mm field of view (FOV). The iPhone capillaroscope developed here has slightly improved on-axis resolution (3.75μm) and a much larger FOV 3.5 x 4.8 mm. Interestingly, blood velocity was not shown necessary for accurate ANC screening in Bourquard et al.'s initial publication, making it possible that sequentially-acquired RAW images on a mobile phone could be used instead of high speed video imaging.

Biomedical Optics EXPRESS

In this study, the iPhone X was chosen for convenience. However, we believe that this technique could be generalized to most other modern mobile camera phones, provided a new capillaroscope housing is designed for a given mobile phone. Table 1 compares a few such options. For example, the original reversed lens mobile phone publication demonstrated $\leq 4\mu$m resolution over a 1mm^2 FOV in an iPhone 4S, a now 8-year-old phone. However, this model of iPhone is limited to 30fps video, and higher frame rates were not introduced until the iPhone 6. Inexpensive Android phones also appear compatible with this technique, such as the ~ $ 150 Motorola Moto G7, whose 12 MP f/1.8, 1.25 μm camera is capable of up to 60fps at 1080p resolution [32]. Though not the most inexpensive, an option we believe is worth pursuing is the ~ $500 Huawei P20 Pro, whose 20MP monochrome f/1.6 camera would be ideal for the quasi-monochromatic illumination used in capillaroscopy. Camera specifications and prices were compiled from *GSMarena.com* and *Newegg.com* as of October 2019 [32,37].

Table 1. Comparison of Mobile Phone Capillaroscope Options

Phone	Cost	Imaging Speed (fps)	f/#	pixel size (μm)	Sampling Limit (μm)
iPhone 4S	$44	30	2.4	1.4	3.95
iPhone 6	$115	60	2.2	1.5	4.24
iPhone X	$590	240	1.8	1.22	3.45
Motorola G7	$200	60	1.8	1.25	3.54
Huawei P20 Pro	$470	60	1.6	1.00	2.00

Future work towards developing a robust mobile phone capillaroscope capable of white blood cell count screening will include imaging microfluidic capillary phantoms with known ground truth white blood cell concentrations. A similar study to Pablo-Trinidad et al. [13] should be conducted *in vivo* in humans with ground truth complete blood counts. Lastly, neutropenia screening using nailfold capillaroscopy has not been shown effective in individuals with Fitzpatrick skin phototype >4, due to loss of absorption contrast to red blood cells from overlying absorptive melanin in the epidermis. The technique requires further innovation to overcome this bias and become an effective global health tool.

5. Conclusion

Nailfold capillaroscopy is a simple microscopy technique with exciting and unexplored clinical utility. Resolution and quantification of optical absorption gaps (OAGs) in nailfold capillaries *in vivo* has been shown to be an effective tool for neutropenia screening. In this paper, we demonstrate that OAGs can be resolved in nailfolds *in vivo* with a simple add on to a mobile phone. These data lay the groundwork for further clinical studies testing the efficacy of mobile phone capillaroscopy for white blood cell count screening in patients with ground truth complete blood count values. Future work could include the assessment of more sophisticated illumination strategies that may improve phase contrast and specificity to white blood cells [38], as well as a side by side comparison of OAG frequency measured by mobile phone capillaroscopy to WBC count measured by conventional blood draw and laboratory analysis. Due to its portability, affordability, and potential to serve as a screening tool for a conventionally lab-based invasive test, the mobile phone capillaroscope could serve as an important point-of-care tool.

Funding

National Institutes of Health (R21 EB024700, R43 CA228920).

Biomedical Optics EXPRESS

Disclosures

C.C.G., I.B., A.B., and A.S.F. have an issued patent on the proposed technology under patent number US 9,984,277 B2 and title "Systems, Apparatus, and Methods for Analyzing Blood Cell Dynamics". I.B., A.S.F., A.B., and C.C.G. report honoraria, financial support from, and current employment by Leuko Labs Inc. to conduct this research. I.B., A.S.F., C.C.G., and A.B. hold equity in Leuko Labs Inc.

References

1. G. E. Brown, "The Skin Capillaries in Raynaud's Disease," Arch. Intern. Med. **35**(1), 56–73 (1925).
2. F. Lefford and J. Edwards, "Nailfold capillary microscopy in connective tissue disease: a quantitative morphological analysis," Ann. Rheum. Dis. **45**(9), 741–749 (1986).
3. C.-H. Chang, R.-K. Tsai, W.-C. Wu, S.-L. Kuo, and H.-S. Yu, "Use of Dynamic Capillaroscopy for Studying Cutaneous Microcirculation in Patients with Diabetes Mellitus," Microvasc. Res. **53**(2), 121–127 (1997).
4. C. E. Curtis, W. G. Iacono, and M. Beiser, "Relationship between Nailfold Plexus Visibility and Clinical, Neuropsychological, and Brain Structural Measures in Schizoprenia," Biol. Psychiatry **46**(1), 102–109 (1999).
5. P. Jung and F. Trautinger, "Capillaroscopy," J. Ger. Soc. Dermatol. **11**(8), 731–736 (2013).
6. I. Gurov, M. Volkov, N. Margaryants, A. Pimenov, and A. Potemkin, "High-speed video capillaroscopy method for imaging and evaluation of moving red blood cells," Opt. Lasers Eng. **104**, 244–251 (2018).
7. A. Bourquard, A. Pablo-Trinidad, I. Butterworth, Á. Sánchez-Ferro, C. Cerrato, K. Humala, M. F. Urdiola, C. D. Rio, B. Valles, J. M. Tucker-Schwartz, E. S. Lee, B. J. Vakoc, T. P. Padera, M. J. Ledesma-Carbayo, Y.-B. Chen, E. P. Hochberg, M. L. Gray, and C. Castro-González, "Non-invasive detection of severe neutropenia in chemotherapy patients by optical imaging of nailfold microcirculation," Sci. Rep. **8**(1), 5301 (2018).
8. U. Baran, L. Shi, and R. K. Wang, "Capillary blood flow imaging within human finger cuticle using optical microangiography," J. Biophotonics **8**(1-2), 46–51 (2015).
9. G. W. Schmid-Schonbein, S. Usami, R. Skalak, and S. Chien, "The Interaction of Leukocytes and Erythrocytes Capillary and Postcapillary Vessels," Microvasc. Res. **19**(1), 45–70 (1980).
10. S. H. Sinclair, M. Azar-Cavanagh, K. A. Soper, R. F. Tuma, and H. N. Mayrovitz, "Investigation of the Source of the Blue Field Entoptic Phenomenon," Investig. Ophthalmol. Vis. Sci. **30**(4), 668–673 (1989).
11. A. Uji, M. Hangai, S. Ooto, K. Takayama, N. Arakawa, H. Imamura, K. Nozato, and N. Yoshimura, "The Source of Moving Particles in Parafoveal Capillaries Detected by Adaptive Optics Scanning Laser Ophthalmoscopy," Invest. Ophthalmol. Visual Sci. **53**(1), 171–178 (2012).
12. T. Rimmer, E. M. Kohner, and J. M. Goldman, "Retinal Blood Velocity in Patients with Leukocyte Disorders," Arch. Ophthalmol. **106**(11), 1548 (1988).
13. A. Pablo-Trinidad, I. Butterworth, M. J. Ledesma-Carbayo, T. Vettenburg, A. Sanchez-Ferro, L. Soenksen, N. J. Durr, A. Munoz-Barrutia, C. Cerrato, K. Humala, M. F. Urdiol, C. Del Rio, B. Valles, Y.-B. Chen, E. P. Hochberg, C. Castro-González, and A. Bourquard, "Automated detection of neutropenia using noninvasive video microscopy of superficial capillaries," Am. J. Hematol. **94**(8), E219–E222 (2019).
14. E. Tai, G. P. Guy Jr., A. Dunbar, and L. C. Richardson, "Cost of Cancer-Related Neutropenia or Fever Hospitalizations, United States 2012," J. Oncol. Pract. **13**(6), e552–e561 (2017).
15. T. Honda, T. Uehara, G. Matsumoto, S. Arai, and M. Sugano, "Neutrophil left shift and white blood cell count as markers of bacterial infection," Clin. Chim. Acta **457**, 46–53 (2016).
16. J. Crawford, D. C. Dale, and G. H. Lyman, "Chemotherapy-Induced Neutropenia. Risks, consequences, and new directions for its management," Cancer **100**(2), 228–237 (2004).
17. M. B. Lustberg, "Management of Neutropenia in Cancer Patients," Clin. Adv. Hematol. & Oncol. **10**, 825–826 (2012).
18. K. M. Syed and R. S. Pinals, "Leukocytosis in Rheumatoid Arthritis," J. Clin. Rheumatol. **2**(4), 197–202 (1996).
19. K. J. Ciuffreda and M. Rosenfield, "Evaluation of the SVOne: A Handheld, Smartphone-Based Autorefractor," Optom. Vis. Sci. **92**(12), 1133–1139 (2015).
20. K. M. Rappaport, C. C. McCracken, J. Beniflah, W. K. Little, D. A. Fletcher, W. A. Lam, and A. L. Shane, "Assessment of a Smartphone Otoscope Device for the Diagnosis and Management of Otitis Media," Clin. Pediatr. (Philadelphia) **55**(9), 800–810 (2016).
21. R. G. Mannino, D. R. Myers, E. A. Tyburski, C. Caruso, J. Boudreaux, T. Leong, G. D. Clifford, and W. A. Lam, "Smartphone app for non-invasive detection of anemia using only patient-sourced photos," Nat. Commun. **9**(1), 4924 (2018).
22. H. Zhu, O. Yaglidere, T.-W. Su, D. Tseng, and A. Ozcan, "Cost-effective and compact wide-field fluorescent imaging on a cell-phone," Lab Chip **11**(2), 315–322 (2011).
23. Z. J. Smith, K. Chu, A. R. Espenson, M. Rahimzadeh, A. Gryshuk, M. Molinaro, D. M. Dwyre, S. Lane, D. Matthews, and S. Wachsmann-Hogiu, "Cell-Phone-Based Platform for Biomedical Device Development and Education Applications," PLoS One **6**(3), e17150 (2011).

Biomedical Optics EXPRESS

24. I. I. Bogoch, J. R. Andrews, B. Speich, J. Utzinger, S. M. Ame, S. M. Ali, and J. Keiser, "Short Report: Mobile Phone Microscopy for the Diagnosis of Soil-Transmitted Helminth Infections: A Proof-of-Concept Study," Am. J. Trop. Med. Hyg. **88**(4), 626–629 (2013).
25. D. N. Breslauer, R. N. Maamari, N. A. Switz, W. A. Lam, and D. A. Fletcher, "Mobile Phone Based Clinical Microscopy for Global Health Applications," PLoS One **4**(7), e6320 (2009).
26. A. Skandarajah, C. D. Reber, N. A. Switz, and D. A. Fletcher, "Quantitative Imaging with a Mobile Phone Microscope," PLoS One **9**(5), e96906 (2014).
27. N. A. Switz, M. V. D'Ambrosio, and D. A. Fletcher, "Low-Cost Mobile Phone Microscopy with a Reversed Mobile Phone Camera Lens," PLoS One **9**(5), e95330 (2014).
28. E. J. Botcherby, R. Juskaitis, M. J. Booth, and T. Wilson, "An optical technique for remote focusing in microscopy," Opt. Commun. **281**(4), 880–887 (2008).
29. WHO, "The top 10 causes of death," https://www.who.int/news-room/fact-sheets/detail/the-top-10-causes-of-death (2019).
30. D. S. Chabot-Richards and T. I. George, "Leukocytosis," Int. Jnl. Lab. Hem. **36**(3), 279–288 (2014).
31. Fixez, "iPhone X Dual Rear Camera Replacement - SKU# 9-AP-3772," https://www.fixez.com/catalog/product/view/id/2924/s/iphone-x-dual-rear-camera-replacement/ (2019).
32. GSM, "GSM Arena," https://www.gsmarena.com/ (2019).
33. G. N. McKay, T. L. Bobrow, S. Kalyan, S. C. Hur, and N. J. Durr, "Optimizing white blood cell contrast in graded-field capillaroscopy using capillary tissue phantoms," in *Proc. SPIE 11243, Imaging, Manipulation, and Analysis of Biomolecules, Cells, and Tissues XVIII*, (2020).
34. C. Mitja, "Slanted Edge MTF," https://imagej.nih.gov/ij/plugins/se-mtf/index.html (2011).
35. C. E. Shannon, "Communication in the Presence Noise," *Proc. I.R.E.* pp. 10–21 (1949).
36. A. Bollinger, P. Butti, J. P. Barras, H. Trachsler, and W. Siegenthaler, "Red blood cell velocity in nailfold capillaries of man measured by a television microscopy technique," Microvasc. Res. **7**(1), 61–72 (1974).
37. Newegg, "Newegg," https://www.newegg.com/ (2019).
38. G. N. McKay, N. Mohan, and N. J. Durr, "Imaging human blood cells in vivo with oblique back-illumination capillaroscopy," arXiv **2001.06284** (2020).